Computers and Chemical Engineering 161 (2022) 107767

Contents lists available at ScienceDirect

Computers and Chemical Engineering

journal homepage: www.elsevier.com/locate/compchemeng

Computer simulation to optimize roller screen settings providing higher efficiency in green pellets classification

Akbar Jafari[a,*], Meisam Javaheri[b], Gholamhosein Baradaran[b]

[a] Department of Mechanical Engineering, Technical and Vocational University (TVU), Tehran, Iran
[b] Department of Mechanical Engineering, Faculty of Engineering, Shahid Bahonar University of Kerman, P.O. Box: 7616913439, Kerman, Iran

ARTICLE INFO

Article history:
Received 8 August 2021
Revised 15 February 2022
Accepted 8 March 2022
Available online 10 March 2022

Keywords:
DEM
Computer simulation
Roller screen
Optimization
Efficiency
Green pellet

ABSTRACT

DEM computer simulation was implemented to reveal the effects of different parameters on the efficiency of the roller screen. The numerical simulations were conducted under different device settings. In addition to the overall efficiency, further index was defined to determine the portion of cooperation of the rollers with different locations along the length of the device. It was revealed that the increase in the deck angle and rollers diameter reduced the overall efficiency while there was an optimum speed delivering the highest efficiency. It was concluded that the local cooperation share also depends on the introduced factors. In addition to the efficiency as an operational aspect, mechanical strength criteria were also considered to avoid probable device failure. Discussions were drawn concerning the obtained results and probable physical reasons of the obtained dependencies. The results can assist pelletizing factories to reduce their overall cost owing to increasing the process efficiency.

1. Introduction

Iron and its alloys are the most important engineering materials utilized in industries. After the Second World War, the demand for all engineering materials was increased rapidly, with iron still ranking first. There are different approaches to obtaining metallic iron from iron ore concentrate including blast furnace and direct reduction. In the blast furnace technology, powdered iron ore concentrate with a size of tens of microns is charged into the furnace. On the other hand, in the reduction process the charge into the reactor is in the form of pellet. Via chemical reactions between the charged natural gas and the iron pellet in the reactor, oxygen is eliminated from either Hematite (Fe_2O_3) or Magnetite (Fe_3O_4) to obtain pure iron (Fe). Such process results in iron sponges suitable for subsequent melting and casting process. The diameter of the pellets should be in a certain range, preferably 8-16 mm, to have a successful reaction in the direct reduction process. Therefore, iron pellet is the main requirement for making sponge iron, and is made via the agglomeration of iron ore small particles in a rotating drum or rotating disk (flange on the rim). The agglomeration occurs due to different reasons including the surface tension of the water around the particles, adhesion of the binder, wan der Waals forces, magnetic force associated with the paramagnetic property of the particles and physical interlocking of the particles. The green pellets produced in the balling drum/disk are sent into the induration furnace to be heated up to 1300 °C and then cooled down to the ambient temperature. The objective of the present research is studying the screening process of the green pellets prior to feeding the induration furnace; thus, for more illustrations about other processes, interested readers can refer to relevant references such as Tupkary and Tupkary (2013).

The diameter (size) of the green pellets fed into the induration furnace should be in a range suitable for the sintering process. If the pellets are smaller than an acceptable limit, permeability is reduced and the burning gas cannot flow along the depth of the pellets layer. On the contrary, if the pellets are larger than a specific limit, sintering does not happen completely and the quality becomes inacceptable for the reduction stage. The green pellets produced in the balling drum/disk are generally in various rather than a certain size. There are several parameters in pelletizing drum/disk which influence the mechanical properties and sizes of the produced green pellets. Due to the importance of the mechanical characteristics and size of the pellets, several theoretical and experimental studies related to the pelletizing stage have been conducted by researchers and industries (Kotta et al., 2019; Nyembwe et al., 2017). One of the practical approaches proposed and implemented in a few industrial sites is on-line control via image processing using intelligent systems (Halt et al., 2015; Hamzeloo et al., 2014; Heydari et al., 2016). In that method, currently implemented in Golgohar pellet factory (http://www.geg.ir/, 2019), the pictures of the produced pellets in the balling disk are

* Corresponding author.
E-mail address: a_jafari@tvu.ac.ir (A. Jafari).

https://doi.org/10.1016/j.compchemeng.2022.107767
0098-1354/

analyzed to find their size distribution. Based on the correlation between the size distribution and tunable factors such as the rotating speed, necessary adjustments are done to improve the size distribution. However, the environment around the balling drum/disk is not generally clean, hence the issues caused by the pollution in cameras make some difficulties in image processing. Moreover, there are several parameters that affect the balling process, while few of them can be adjusted. Furthermore, there is a lag between the time that a parameter in a production line is changed and the time its impact is exhibited. As another important fact, optimization of green pellet is a two-objective optimization problem in which the pellets should simultaneously have optimum size and optimum mechanical strength. Nevertheless, setting a parameter (e.g. disk speed) might lead the pellets size distribution to the optimum range, but does not necessarily maintain the mechanical strength in the acceptable range. These explanations indicate that the problem of achieving the optimum pellets in the pelletizing unit has not been completely solved and producing pellets in a wide size range in the pelletizing stage seems to be unavoidable. Nevertheless, pellets with optimum size and mechanical properties should be charged into the induration furnace. Currently, screening the green pellets prior feeding to the induration furnace is a practical solution which guaranties achievement of optimum pellets in terms of size distribution. Accordingly, the green pellets with on-size distribution are transferred to the furnace and those with out of size range return to the pelletizing unit.

In the past, vibrating screens were employed to classify the green pellets, which caused their breakage and deformation problem. In 1990 decade, roller screens were introduced as they have reasonable efficiency and induce less damage to the green pellets. Nowadays, roller screen is a vital device in all pelletizing factories around the world. Moreover, this device is employed for the sorting of agriculture products, fruits and waste classification (Hyvärinen et al., 2020; Sofu et al., 2016). Although many studies related to vibrational screens have been reported in the literature, the works pertaining to roller screens are few (e Silva et al., 2018, 2020; Javaheri et al., 2021; Yang et al., 2020). The short application history of this device might be one of the reasons for such paucity of the reported relevant research. In addition to the difficulties of implementing experimental approaches, the cohesive nature of pellets is a challenging issue that hasn't fully comprehended, particularly for implementation in numerical approaches such as the discrete element method (DEM). A variety of studies have been carried out in different fields with DEM, confirming its capability in scientific and industrial aspects (Cleary, 2010; Yu et al., 2018). The work of Cundall and Strack (1979) is among the first reports on the application of DEM in studying particulate materials. This method has been used to reveal the role of influential parameters in vibrating screens (Jafari and Saljooghi Nezhad, 2016; Wang et al., 2019). Although the original version of DEM is limited to the study of circular/spherical particles, modeling of irregular particles is under development and noticeable advancements have been reported (Cleary, 2019; He et al., 2018). DEM has further been implemented in studying the wear of surfaces that work in particulate media (Jafari and Abbasi Hattani, 2020; Jafari and Saljooghi Nezhad, 2016; Powell et al., 2011).

In Yang et al. (2015) DEM is employed to model softening and melting of wax balls as representative of ore particles. DEM has also been employed in the agglomeration of particles (Mishra et al., 2002), where the JKR model (Johnson et al., 1971) has been used in a 2-D simulation of pelletizing 5000 particles inside a rotating drum. Based on the results of that research, agglomeration depends on the particles impact velocity; and the dependence on the velocity varies with the viscosity of the interphase between the particles. Three-dimensional discrete element method was employed to simulate the blast furnace in order to study the effects of particle diameter and coke layer thickness on the solid flow and stress distribution (Geleta and Lee, 2018). DEM has also been employed to simulate crushing in which the particles are broken into smaller ones (Liu et al., 2018; Tavares, 2017). In such problems, the energy of the impact is calculated and breakage is identified based on the breakage rate function. That function depends on the size and mechanical properties of the particle.

The above literature review proves that DEM is a suitable approach for computer simulation of different devices and processes that deal with particulate materials. Moreover, there is a lack of research regarding roller screens despite its necessity for the relevant industries. EDEM software has been employed in several case studies successfully (Ghodki et al., 2019; https://www.edemsimulation.com, EDEM, 2018) and is used here to conduct the required simulations (Solutions, 2018).

2. Theory and formulation

In a particulate medium, resultant force $\vec{F}_i$ and moment $\vec{M}_i$ on ith particle causes the motion described via the following equations:

$$\frac{\partial^2 \vec{r}_i}{\partial t^2} = \frac{1}{m_i}\vec{F}_i \tag{1}$$

$$\frac{\partial^2 \vec{\varphi}_i}{\partial t^2} = \frac{1}{J_i}\vec{M}_i \tag{2}$$

In the above equations, $\vec{r}_i$ and $\vec{\varphi}_i$ are, respectively, the position and orientation vectors of ith particle with a mass of m_i and moment of inertia J_i. In DEM, the above equations are numerically time integrated to determine the location, velocity and acceleration of the particles.

As a particle strikes another particle or a wall, an interaction force is created at the contact zone. In cases where there is no attraction agent, repulsion occurs when particles touch one another. Different models such as Mindlin-Hertz viscoelastic model have been proposed to estimate the repulsion force between two particles. In these models, the repulsive force is determined based on the overlap, δ, shown in Fig. 1. Nevertheless, in the current problem the pellets contain around 8% moisture creating an attraction force between each particle and its neighbor particles/walls. Therefore, as depicted in Fig. 1 even the particles are not in contact with each other the attraction occurs. This is called cohesive force when the attraction is due to a cohesive agent.

JKR is a suitable model to estimate the interaction force between cohesive particles (Johnson et al., 1971). Based on this model, interaction is a combination of viscoelastic and cohesive forces as follows (Baran et al., 2009).

$$F_{JKR} = \frac{4E^*}{3R^*}a^3 - 4\sqrt{\pi\gamma a^3 E^*} \tag{3}$$

In the above equation, E^* and R^* are equivalent Young's modulus and equivalent particles radius, respectively, obtained from the following equations. Indices 1 and 2 indicate the label of the two colliding particles.

$$\frac{1}{E^*} = \frac{1-\nu_1^2}{E_1} + \frac{1-\nu_2^2}{E_2} \tag{4}$$

$$\frac{1}{R^*} = \frac{1}{R_1} + \frac{1}{R_2} \tag{5}$$

Moreover, a is the radius of the contact zone that is related to the surface energy, γ, as follows.

$$\delta = \frac{a^2}{R^*} - \sqrt{\frac{4\pi\gamma a}{E^*}} \tag{6}$$

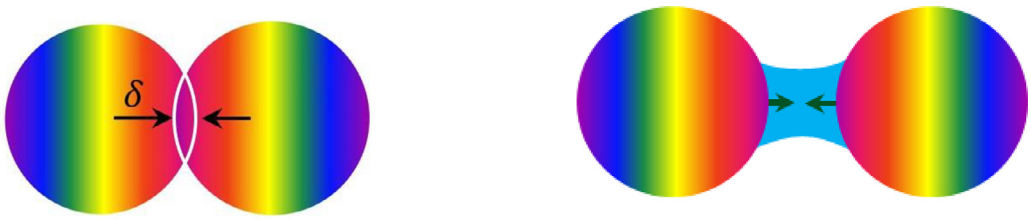

Fig. 1. Exhibition of repulsive force due to physical contact and existence of attraction force due to the moisture cohesion.

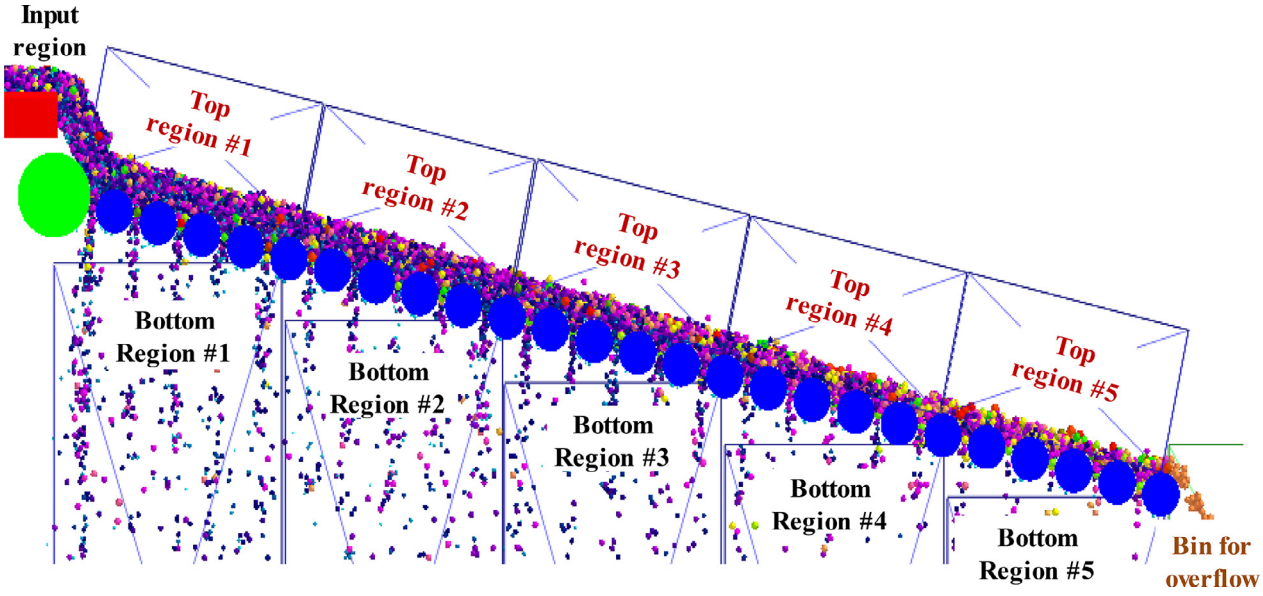

Fig. 2. Collector boxes to measure the pellets mass rate at different regions of the roller screen.

If there is no cohesion between the particles, the variable γ is eliminated and the above equation becomes a geometrical relationship between the interference and radius of the contact zone.

3. Problem description and simulation strategy

The objective of the current research is the simulation of a roller screen for the classification of iron green pellets. The geometry and characteristics of the problem are based upon the installed device before the induration furnace of Golgohar pelletizing plant (http://www.geg.ir/, 2019). As depicted in Fig. 2, the green pellets drop on a belt conveyor from a rectangular region. This conveyor is installed to feed the roller screen and its width is equal to the length of the rollers. Similar to the realistic conditions, pellets drop on a large roller named impact roller, with a diameter of 164 mm. The impact roller is large and strong enough to resist the impact of the pellets dropping from the conveyor with a height of around 0.5 m. In this roller screen, there are N rollers with a diameter of $d_R$installed along the length of the device. As given in Table 1, the length of the screen and the gap between the rollers are, respectively, fixed in values of $L = 2650$ mm and $b = 16$ mm; however, different rollers diameter values lead to different numbers of rollers. The pellets have spherical shapes and their diameters range from 4 mm to 20 mm with detail described in Table 1. To further reveal the role of the deck angle, α, simulations with different values of this parameter were conducted. In the real device, the length of the rollers is $W = 4$ m; however, simulation in this scale entails high computational costs hindering the large simulation number required under different conditions. Thus, the length of the rollers was scaled down to 0.25 m, however, the feed rate per width of the screen was the same as the real condition. All rollers rotate with the same angular speed, ω, whose effect on the screen efficiency was studied via several simulations with different speed values presented in Table 1. Moreover, the physical characteristics of the green pellet, rollers, conveyor and side walls are presented in Table 2 (e Silva et al., 2018). Furthermore, surface characteristics are given in Table 3 (e Silva et al., 2018).

Table 1
General characteristics of the roller screen and the green pellets.

Variable (symbol)	Unit	Value
Screen length (L)	mm	2650
Screen width (W)	mm	250
Deck angle (α)	Deg.	8, 12, 18
Rollers diameter (d_R)	mm	60, 85, 100
Rollers number (N)	-	34, 26, 23
Gap (b)	mm	16
Rollers speed (ω)	rpm	50, 80, 130, 200, 250, 300, 400
Pellets diameter, d_P, and (share in %)	mm and (%)	4 ~ 6.25(0.4), 6.25 ~ 8(0.8), 8 ~ 10 (5.0), 10 ~ 12.5(40.6), 12.5 ~ 14(32), 14 ~ 16(16.6), 16 ~ 20(4.6)
Feed rate ($\dot{m}$)	kg/s	17.5
Time step size	μs	14.325, 28.65, 57.303, 114.607

Table 2
Physical characteristics of the green pellets and the screen components.

Property (symbol)	Unit	Pellets	Rollers (steel)	Belt conveyor	Side walls (steel)
Density (ρ)	kg/m^3	3150	7800	860	7800
Shear modulus (G)	N/mm^2	1.8	77200	7.1	77000
Poisson's ratio (ϑ)	-	0.25	0.25	0.25	0.25

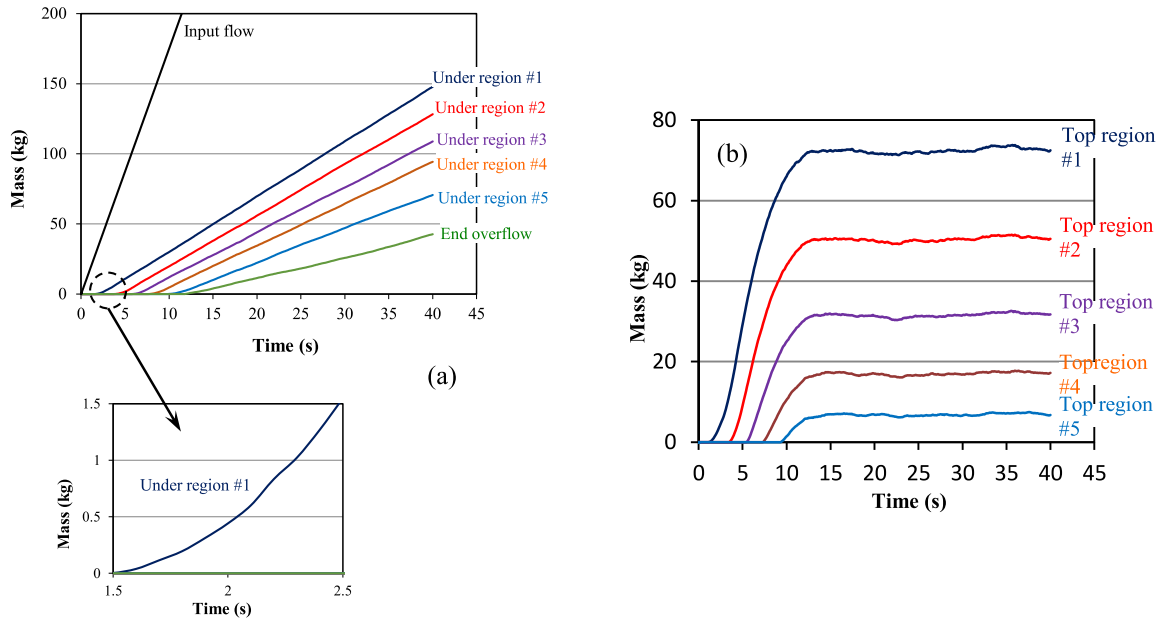

Fig. 3. Graphs of mass-time in (a) input, end overflow and five under screen regions; (b) five underflow regions (settings: $d_R = 60$ mm, $\alpha = 8°$, $\omega = 130$ rpm).

Table 3
Properties of the contacting surfaces.

Property (symbol)	Unit	Pellet-Pellet	Pellet-Roller	Pellet-conveyor	Pellet-Walls
Friction coefficient (μ_s)	-	0.3	0.35	0.71	0.0
Roller friction coefficient (μ_r)	-	0.1	0.25	0.5	0.0
Restitution coefficient (ε)	-	0.05	0.08	0.05	0.08
JKR surface energy (γ)	J/m^2	1.5	0.5	0.5	0.0

Although several factors affect the roller screen efficiency, effects of the rollers diameter, rollers rotational speed and deck angle on the device efficiency were selected to be studied as they can be changed/tuned in practical conditions. For this purpose, several simulations were conducted for different values of these variables as presented in Table 1. From now on, when the value of a variable is not declared, its base value is in purpose which is recorded in bold font in the table. As the gap between the rollers is fixed at $b = 16$ mm, the device function is to let the pellets smaller than this size, called undersized, go under the screen which is named underflow. The pellets size distribution in the feed of the screen is presented in Table 1. The screen overall efficiency, η, is computed by means of the following equation defined as the ratio of the undersized pellets in the underflow to the total undersized pellets existing in the feed.

$$\eta\ (\%) = 100\frac{Undersized\ mass\ rate\ in\ the\ underflow}{Total\ undersized\ mass\ rate\ in\ the\ input\ \ feed} \tag{7}$$

Although the overall efficiency is an important index in studying the performance of the roller screen, the local underflow rate was also studied. As illustrated in Fig. 2, twelve virtual collector boxes were installed at proper locations to compute the pellets number and amount of mass in different locations. The first and last boxes are located at the input and end region of the roller screen. The other ten boxes are located along the length of the device, five over and five below the rollers. The summation of all pellets in the five boxes below the screen gives the total undersized pellets separated from the whole batch. Comparing the mass rate of each region, the parts that participate more in the classification process are revealed. Furthermore, the local mass rate is used to estimate the cooperation index from Eqs. (8) and (9). This index is beneficial to understand how the screening function is done along the length of the screen.

$$Cooperation\ (\%) = 100 * \left(1 - \sqrt{\sum_{i=1}^{5}\left(\eta_i^* - 0.2\right)^2}\right) \tag{8}$$

$$\eta_i^* = \frac{Undersized\ mass\ rate\ in\ region\ i}{Total\ undersized\ mass\ rate\ in\ the\ underflow} \tag{9}$$

η_i^* in Eq. (9) is the share of region i. According to Eq. (9), if all rollers located along the length of the screen have the same contribution in the screening process (uniform cooperation), all values of η_i^* turn out to be 0.2 and cooperation index becomes 100%.

3.1. Steady state condition

If the simulation time is not long enough, the data extraction will be accompanied by an error, hence it is desirable to compute the mass rates in the steady state condition. The screen is considered as a control volume and the following equation represents the mass conservation under the steady state condition. In this equation, $\dot{m}_{in}$ is the feed mass rate, $\dot{m}_{ui}$ $(i = 1 \sim 5)$ is underflow mass rate at region i and $\dot{m}_o$ is the overflow mass rate at the top end of the screen.

$$\dot{m}_{in} = \dot{m}_{u1} + \dot{m}_{u2} + \dot{m}_{u3} + \dot{m}_{u4} + \dot{m}_{u5} + \dot{m}_o \tag{10}$$

The time derivative of the mass-time function, $m(t)$, for each region, gives the mass rate, $\dot{m}$, in/out of that region. If the graph of $m(t)$ for a region is linear, its time derivative is constant which represents a steady state condition. For instance for a specific screen setting, mass-time graphs for the input region, the end region and five regions under the screen are plotted in Fig. 3a. It is observed that as the time passes, the mass in all regions increases non-linearly during the initial period; however, all graphs gradually become linear, meaning reaching the steady state condition. It is further seen that the graph belonging to the input feed becomes linear fast, while the graph of the end region becomes linear later than others. The graphs belonging to the five under regions are plotted in Fig. 3b. It is seen that during the transient condition they vary non linearly with time, while gradually becoming almost plateau. The graphs in the steady state condition are not

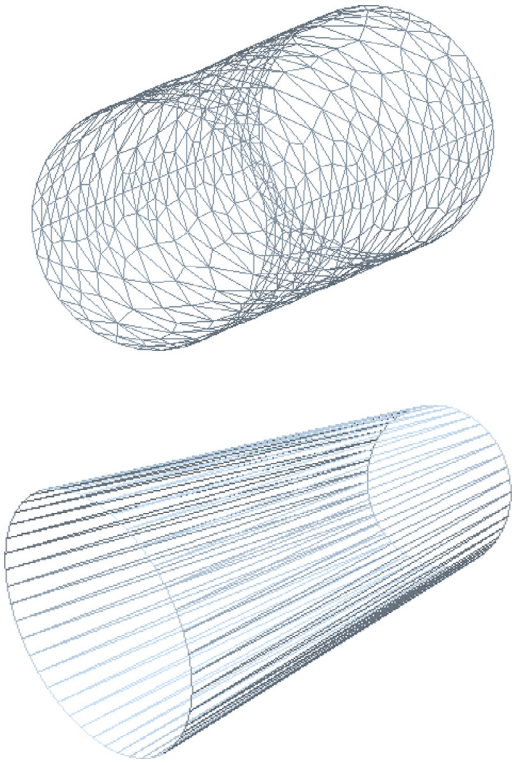

Fig. 4. Two options of the roller surface meshing, by equilateral and narrow isosceles triangular elements.

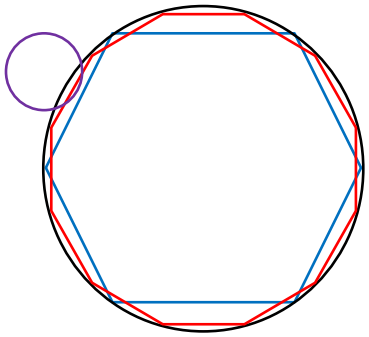

Fig. 5. Different pellet-roller interference detection in two roller meshing size.

completely flat, and there are some small fluctuations expected to be relevant to the transient local gap blockages. It should be insisted that the time when the steady state occurs is not the same in all simulations. However, a period of 40 s is sufficient to reach the steady state condition in all simulations.

3.2. Ensuring the simulation accuracy

Several factors affect the accuracy of a numerical simulation (Danby et al., 2013; Kruggel-Emden et al., 2008). Mesh size of the surfaces, integration time step and domain grid size, or in other words, neighbor list are the important factors that affect the accuracy of the current DEM simulations. In DEM, the real curved surfaces are approximated by triangular elements. In fact, this is similar to domain meshing in the finite element method (FEM). In DEM implementation, coordinates of the element nodes are used in order to compute the location of the element and its unit normal vector at points that are in contact with the particles. As previously mentioned, the unit normal vectors are used to calculate the interaction forces. In the current problem, the rollers are the main parts and their meshing significantly affects the simulation accuracy. As indicated in Fig. 4, two options were followed, namely homogenous (almost equilateral) triangle and narrow (isosceles) triangle. By using the equilateral triangle, the roller surface is discretized in both circumferential and longitudinal directions, while in isosceles shape it is only discretized along the circumferential direction. As there is no curvature along the roller length, discretization along the length is not as important as the circumference.

To clarify the importance of the circumferential meshing on the simulation, the meshing of the roller with two different sizes is presented in Fig. 5. Although the pellet is at the same location, the detected interference depends on the meshing size which can lead to different numerical results. It is obvious that the finer the meshing, the more accurate the results; however, the increase in the number of elements elevates the computational cost. Here, a few simulations were conducted and a proper meshing was selected in a way that the results became almost insensitive to the meshing, and more fining did not considerably affect the results.

Integration time step size is another factor that influences the simulation accuracy. If the time step size is too large, some important parts of the real working time might be lost, while reducing the time step size increases the computational cost. In this research, several simulations were conducted through selection of different time step values. In fact, the selected time step sizes were different ratios of the Rayleigh time step (https://www.edemsimulation.com, EDEM, 2018; O'Sullivan and Bray Jonathan, 2004). To reveal the effects of the time step, overall efficiency, local mass rate and pellets flow regime were extracted and compared. It was seen that all of them vary with the time step; nevertheless, by decreasing the time step size, these dependencies were weakened. As an example for a specific simulation case, variation of the overall underflow rate versus the time step size is given in Fig. 6a. It is observed that when the time step becomes smaller than 28.6 μs, no considerable change happens, and convergence is achieved. Moreover, the pictures in Fig. 6b and c show the flow regime for a large and a proper size of the time step. It is seen that for the large time step size, a non-realistic flow regime is happened, while a uniform flow regime is occurred in the case of using a proper time step. Accordingly, the value of 14.3 μs was selected to conduct the simulations. It should be noted that although the materials were identical in all simulations, the convergence was also dependent on other factors, especially the size and speed of the rollers. Here, a few computers were used to conduct the simulations. In case of using a system with characteristics of Processor: 6 Core, 2.8 GHz, 12 MB L3 Cache, 95 W, DDR3-1333, HT, Turbo, Memory: 64 GB DDR3, it takes around 50 h to run a typical simulation. However, simulation time depends on the problem settings. For example, when the deck angle is small, number of pellets stacked on the screen increases causing creation of further contact points and requiring more computational effort consequently.

4. Numerical results and discussion

As depicted in Fig. 7 the pellets can be categorized into four groups including: 'Much undersized' that are much smaller than the gap between the rollers and creates the least trouble for passing through the gap and therefore this group takes critical degree of 1. The pellets that are much larger than the gap, named 'Much oversized', stay on top of the batch and do not remain inside the trap between the rollers and they can travel to the end of the screen with minor trouble and hence are categorized as critical degree of 2. The pellets that are slightly smaller than the gap named 'Near undersized' have a high probability of coming inside the trap between the rollers. They can pass through the gap although not easily and hence take critical degree of 3. The pellets a little larger than the gap named "Near oversized", and create the most serious

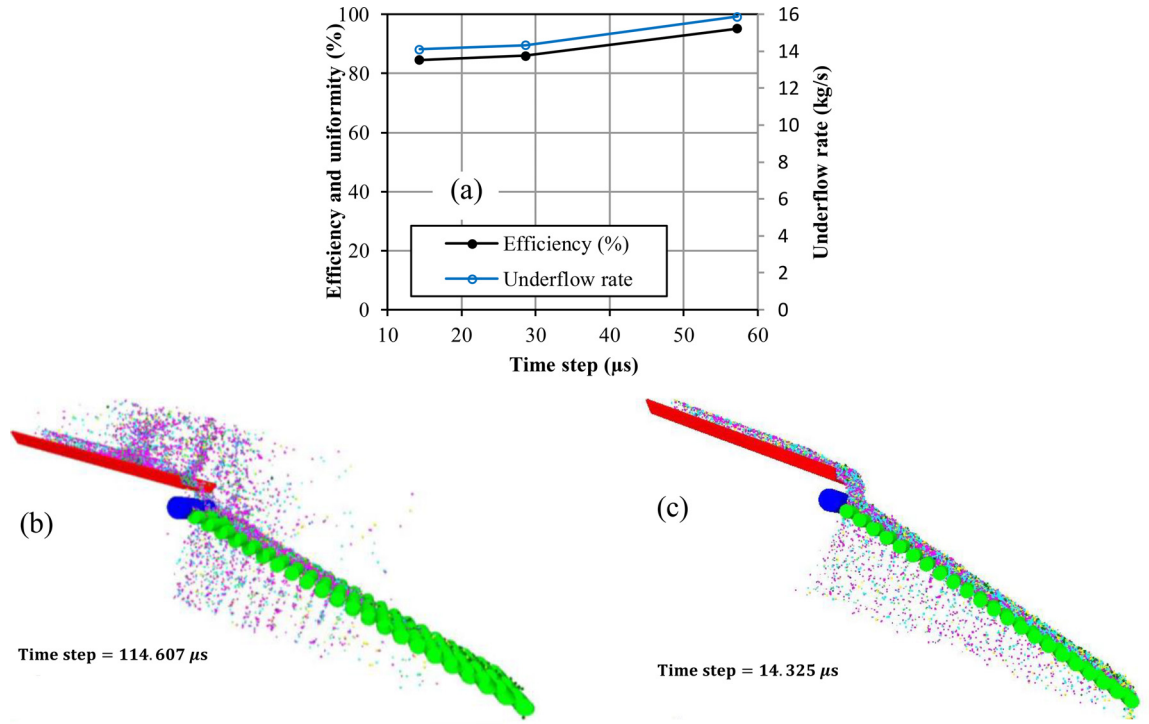

Fig. 6. Dependence of the results on the time step size; (a) Total efficiency, (b) Perturbed flow regime due to selection of a large time step and (c) Uniform flow due to selection of a suitable time step. (Simulation case: $d_R = 100$ mm, $\alpha = 12°$, $\omega = 200$ rpm).

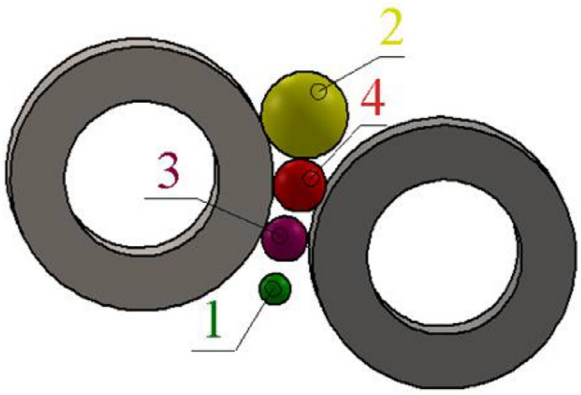

Fig. 7. Four sizes of the pellets from the least critical to the most critical situation for blinding of the gap between the rollers.

problem for the screen as they remain inside the trap between the rollers similar to a wedge causing blinding the gap. Therefore, the highest critical degree, 4, is assigned to this group of pellets.

Clearly, the size of a trapped pellet is the key factor for defining the magnitude and direction of the contact forces. Actually, when the pellet size is closer to the gap size, makes more significant problem for the screen. However, the rollers size, the rollers speed and the deck angle influence the magnitude and direction of the interaction forces and the screen efficiency consequently. In the coming subsections, direct and cross effects of these factors on the screening process are presented and discussed.

4.1. Rollers with diameter of 60 mm

For specific conditions of $d_R = 60$ mm, and three values of the deck angle: $\alpha = 8°$, $12°$, and $18°$, graphs of the local mass rate versus the screen length for different values of the rollers speed are plotted in Fig. 8. It is seen that at all speeds and for all the three angles, the share of the first region is higher than the others. The graphs belonged to different values of the deck angle indicates that by increasing the deck angle the graphs shift down, meaning decrease in the underflow rate. Another deduction of these graphs is revealing the cross dependence of the efficiency on the rollers speed and the deck angle. In this regard, it is observed that by increasing the deck angle, the graphs belonged to the higher speeds shifted down intensely. For instance, by increasing the deck angle, the graph of 400 rpm approaches zero.

The graphs of the efficiency and cooperation index concerning to $\alpha = 8°$, $12°$, $18°$ are plotted in Fig. 9. The graphs of the efficiency reveal that by increasing the rollers speed, firstly, the screen efficiency increases and then decreases so that the highest efficiency is attained at a specific speed depending on the deck angle. In other words, all graphs have an optimum point that shows maximum attainable efficiency. However, as marked by an arrow, the highest attainable efficiency is reduced following the increase in the deck angle, and the optimum speed goes to a lower value. Furthermore, it is seen that for small deck angle of $\alpha = 8°$ the cooperation index is almost unchanged. However, by increasing the deck angle, the dependence of the cooperation index on the rollers speed is intensified such that it decreases dramatically when the speed is 400 rpm. To confirm these explanations and develop our knowledge on this issue, the problem was further investigated for other values of the rollers diameter. Physical explanations of the relationship between different parameters are postponed to the end of this section when all required studies are conducted.

4.2. Rollers with diameter of 85 mm

The diameter of the rollers was changed to 85 mm and the required simulations were conducted for different values of the rollers speed and deck angle. In Fig. 10, graphs of the local mass rate versus the device length are presented. It is seen that region one has the highest participation in the screening process. It is also seen that for the smaller values of the deck angle, the graph per-

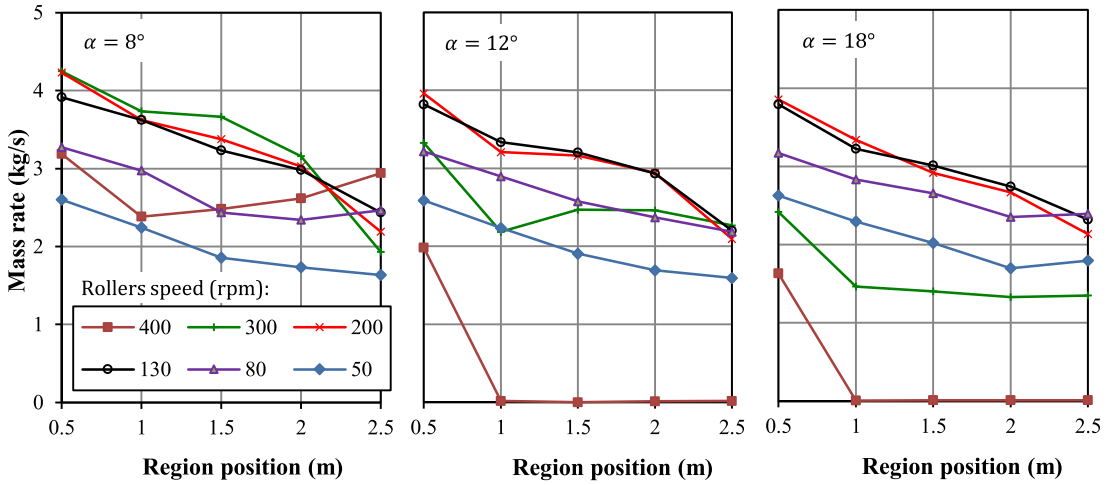

Fig. 8. Underflow mass rate at the five regions along the screen, in case that $d_R = 60$ mm, non-mentioned parameters are at their base values.

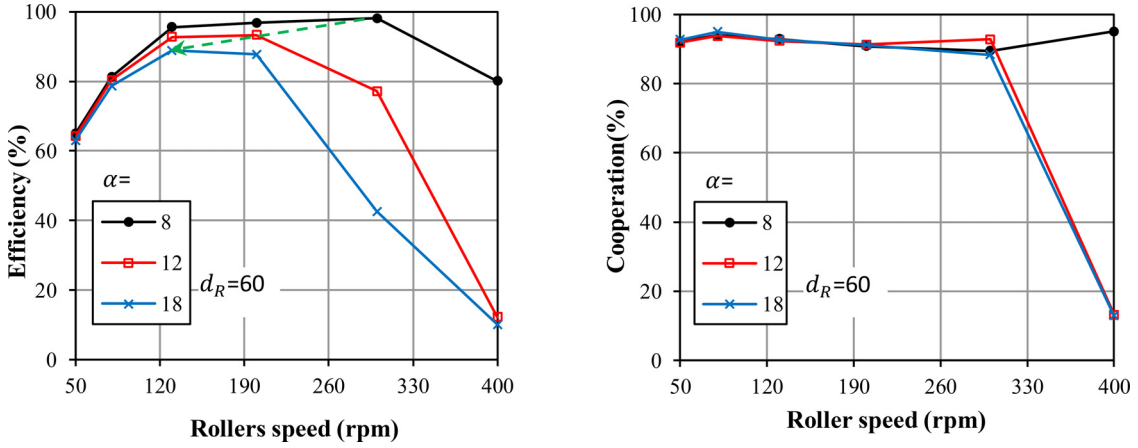

Fig. 9. Efficiency and cooperation index versus the rollers speed in cases of $\alpha = 8°$, 12°, 18° while $d_R = 60$ mm and other parameters are at their base values.

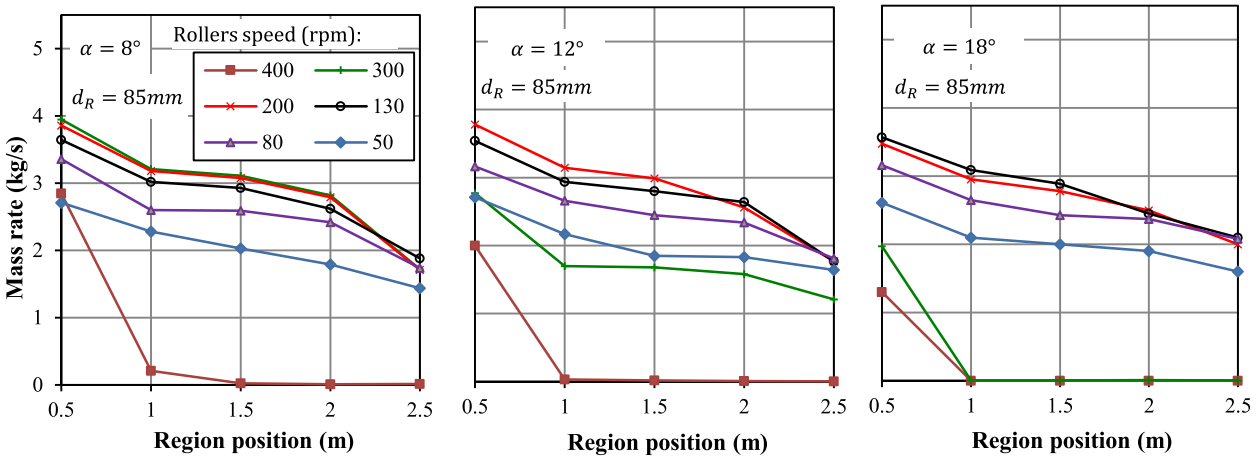

Fig. 10. Underflow mass rate at the five regions along the screen, in case that $d_R = 85$ mm, non-mentioned parameters are at their base values.

taining to the rollers speed of 400 rpm takes the lowest position however, by increasing the deck angle the graph of 300 rpm is also degrades dramatically. This implies that except the first region, the rest of the screen works like a conveyor. On the other hand, for the case of the smallest deck angle, $\alpha = 8°$, the most top graph belongs to 300 rpm, and by increasing the deck angle to $\alpha = 12°$ and then $\alpha = 18°$ the graph of 200 and 130 rpm takes the top rank, respectively.

To determine the optimum rollers speed and how it depends on the deck angle - for rollers diameter of 85 mm - graphs of the efficiency and cooperation index versus the rollers speed are presented in Fig. 11. It is seen that as the deck angle increases, the maximum attainable efficiency decreases. Moreover, it is observed that the optimum speed depends on the deck angle and as shown by the arrow in the figure, this optimum value is reduced by the increase in the deck angle. Furthermore, it is seen that by

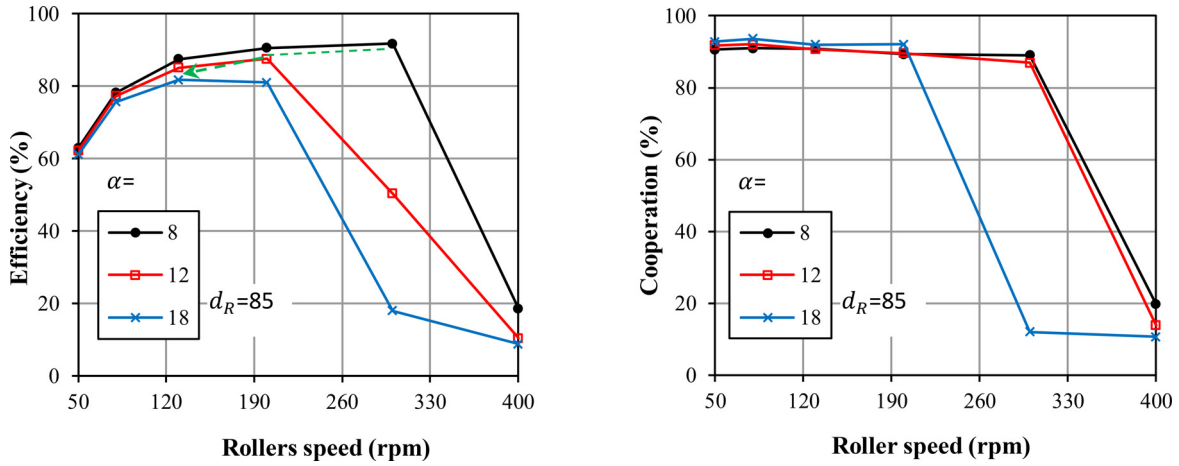

Fig. 11. Efficiency and cooperation index versus the rollers speed in cases of $\alpha = 8°, 12°, 18°$ while $d_R = 85$ mm and other parameters are at their base values.

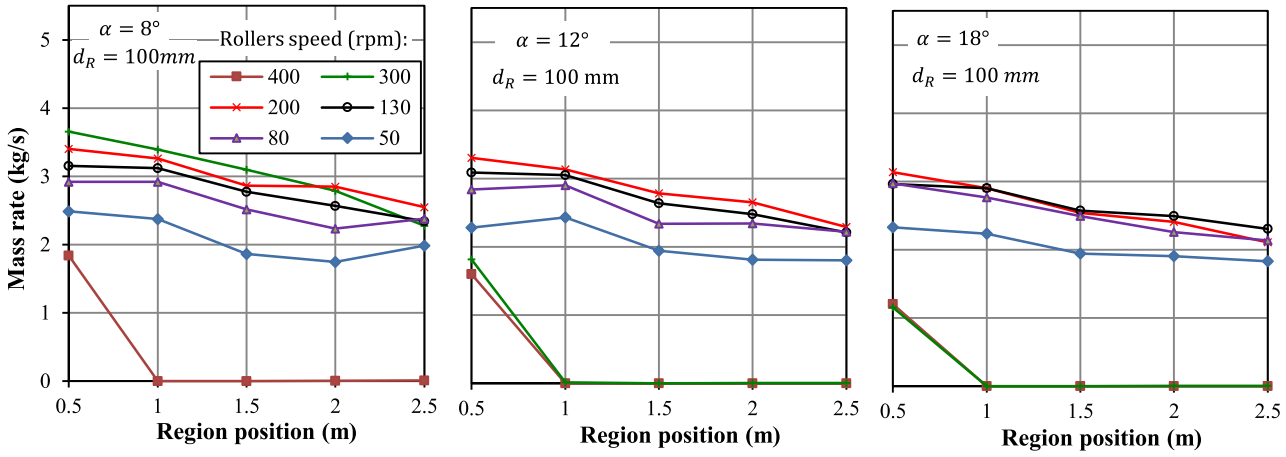

Fig. 12. Underflow mass rate at the five regions along the screen, in case that $d_R = 100$ mm, non-mentioned parameters are at their base values.

increasing the roller speed the cooperation index is reduced and finally dramatically drops. It is observed that by increasing the deck angle, this sudden reduction is occurred at a smaller roller speed. This corresponds to the performance diagrams so that the optimal speed decreases with increasing the deck angle.

4.3. Rollers with diameter of 100 mm

To understand the behavior of the device more comprehensively, simulations of the roller screen with $d_R = 100$ mm were also conducted. Graphs of the local underflow rate are presented in Fig. 12. It is seen that by increasing the deck angle all graphs shift down, meaning decrease in the underflow rate. Furthermore, by increasing the deck angle graphs of the higher speeds drops considerably. In the case of deck angle $\alpha = 8°$ roller speed of 300 rpm takes the highest position while increasing the deck angle to $\alpha = 12°$ roller speed of 200 rpm gets the highest position. By increasing the deck angle to $\alpha = 18°$ the graph of 130 rpm is higher although it is close to the graph of 200 rpm.

For the screen with $d_R = 100$, efficiency and cooperation graphs for different values of the deck angle are plotted in Fig. 13. It is seen that the preferable deck angle is 8° as provides the highest attainable efficiency and angles 12° and 18° gets the next ranks. Furthermore, it is observed that by increasing the deck angle, the optimum speed is reduced. In addition, it is seen that for each value of the deck angle, beyond a specific roller screen the cooperation decays suddenly. Concurrent observation of the local mass rate graphs in Fig. 12 and the cooperation index in Fig. 13 indicates that when the rollers speed goes higher than the optimum value, the cooperation index is degraded as only the first region contributes to the screening process and the others play a conveying role.

4.4. Cross impacts of rollers diameter, rollers speed and deck angle

To realize the effects of the three factors: rollers diameter, rollers speed and deck angle concurrently, adequate graphs and discussions are presented in this subsection. Moreover, the results are compared with the relevant ones reported in e Silva et al. (2020) via the graphs depicted in Fig. 14. It is seen that for different setting conditions, dependency of the efficiency to the deck angle is almost linear similar to the trends reported in e Silva et al. (2020). However, despite the linear dependency on the deck angle, the slope of the graphs depends on the rollers diameter and rollers speed. Similarly, dependency on the rollers diameter is almost linear in the current study and the mentioned reference. Nevertheless, the degree of the linear trend varies depending on the deck angle and rollers speed. Although the current study is conducted for a wide range of the rollers speed, the results were refined in the specific range presented in Fig. 14. It is seen that similar to e Silva et al. (2020), the efficiency-rollers speed graphs are nonlinear with a maximum point exhibited at a definite speed. Without applying optimization procedure, the form of these

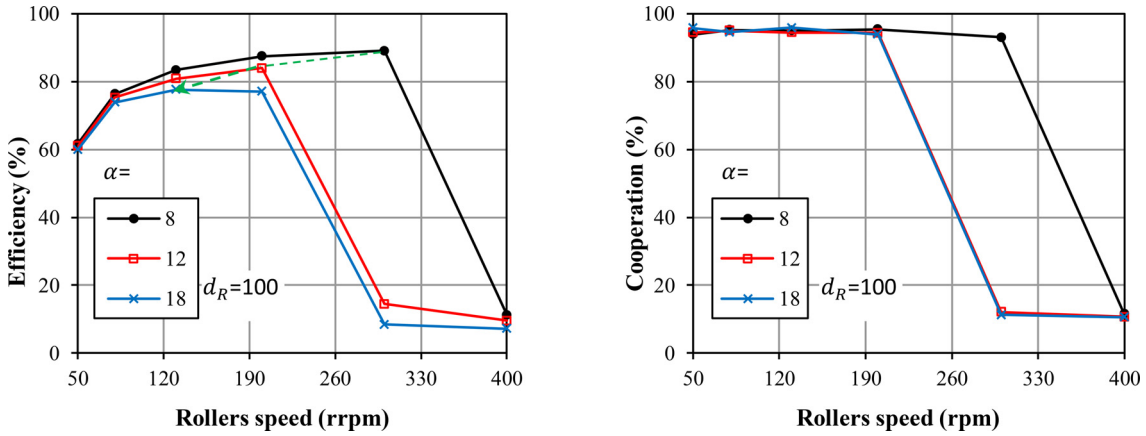

Fig. 13. Efficiency and cooperation index versus the rollers speed in cases of $\alpha = 8°$, 12°, 18° while $d_R = 100$ mm and other parameters are at their base values.

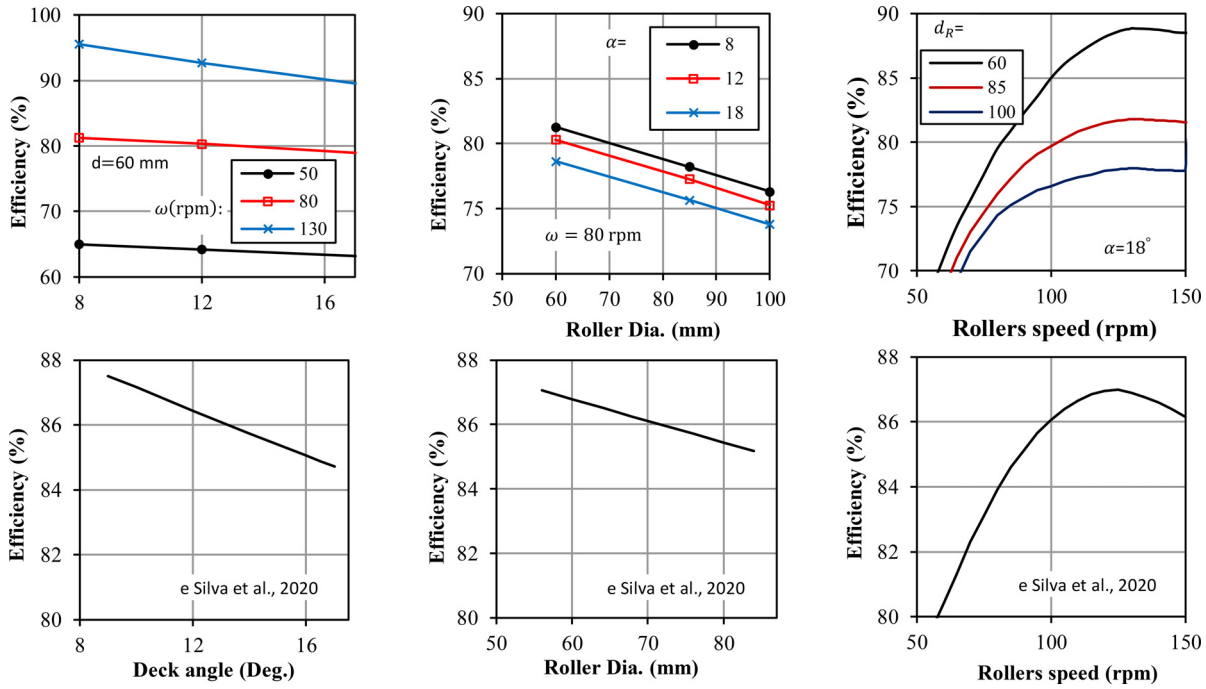

Fig. 14. Comparing the obtained results with the relevant ones reported in e Silva et al. (2020).

graphs lets us conclude that the peak of each graph represents the optimum condition as provides the highest attainable efficiency.

To comprehend relations between the efficiency and the three factors: rollers speed, deck angle and rollers diameter in a wide range, relevant graphs are presented in Fig. 15. It is seen that each graph has its own maximum point, representing the highest attainable efficiency. As indicated by arrows for each deck angle, for all graphs belonging to all rollers diameters the peaks situated at an almost the same speed. Nevertheless, the optimum speed moves to a smaller value with increase in the deck angle. Another outcome of these graphs is that by increasing the rollers diameter, the maximum attainable efficiency decreases. To have more clarity, for three values of the deck angle, the graphs of the highest attainable efficiency versus the rollers diameter are plotted in Fig. 16. This figure reveals that when the deck angle is small, the maximum attainable efficiency increases (though not noticeably) by reducing the rollers diameter. Moreover, at the smallest deck angle ($\alpha = 8°$), the optimum speed is the highest, while after increasing the deck angle to 12° and 18° the optimum speed is reduced. Furthermore, it is seen that by increasing the deck angle, variations of the graphs become more intense, indicating the higher dependency of the maximum attainable efficiency on the rollers diameter. In other words, when the deck angle is increased, the rollers diameter has to be considerably reduced and the rotation speed should be lower in order to obtain the highest achievable efficiency.

To physical explanations for such dependencies, two schematics are presented in Fig. 17. As it is seen from Fig. 17a, by decreasing the deck angle, the effective opening area -shown by arrows- are enlarged leading to enhance the chance of undersize pellets going under the screen and increasing the efficiency. Nonetheless, by decreasing the deck angle, the component of the traction force and the pellet weight along the screen is diminished and therefore the probability for going the near sized pellets out of the trap is decreased leading to blinding and decreasing the efficiency consequently. Therefore, declining the deck angle has both positive and negative effect on the screen efficiency. However, based on the numerical results obtained here, declining the deck angle provided higher efficiency meaning that its positive impact is stronger than its negative role. Furthermore, as shown in Fig. 17b, by decreasing the rollers diameter, the wedge shape trap between the rollers

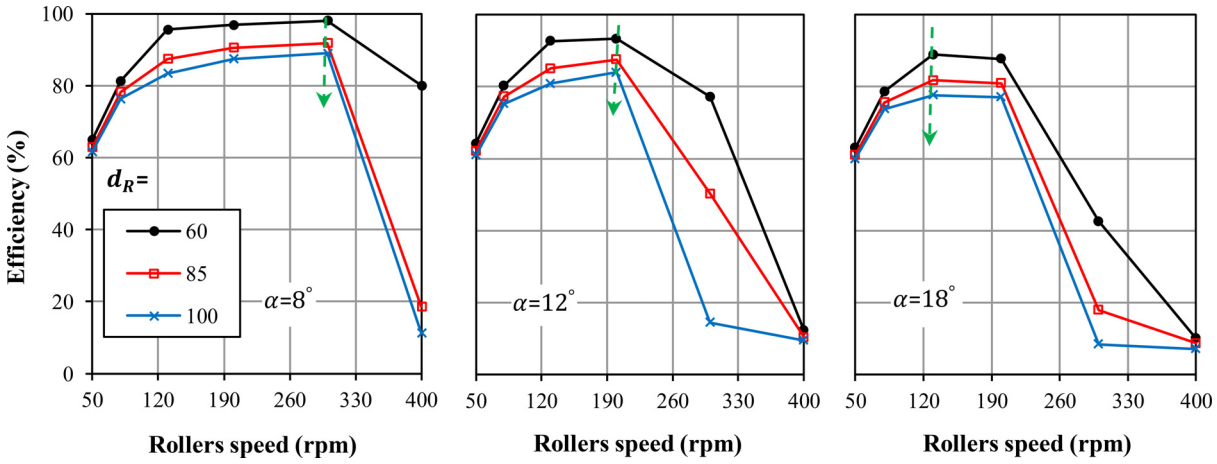

Fig. 15. Dependency of the efficiency versus the rollers speed for different values of the deck angle and rollers diameter.

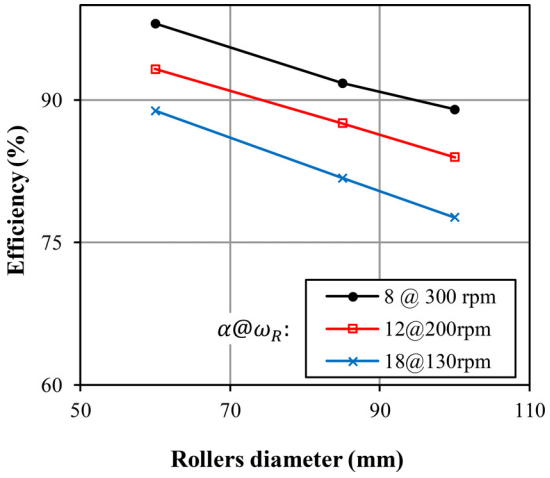

Fig. 16. The highest attainable efficiency versus the rollers diameter and associated optimum speed.

is shortened and therefore fewer pellets might remain in this region, and the probability of blinding is reduced. This is in consistent with the obtained numerical results as it was seen that by decreasing the rollers diameter the efficiency was increased. In addition, it should be insisted that decreasing the rollers diameter provides a possibility to have more rollers and more gaps along the screen leading to enhance the screen efficiency. Pertaining the effects of the rollers speed, it can be urged that has two opposite effects. A positive impact is due to increasing power of the traction force as it depends on the speed of its action point. The negative influence of the rollers speed is lessening of the time that pellets retain on the screen due to increasing of the pellets speed. Based upon the obtained numerical results in the current study, there is an optimum speed showing that in speeds less or more than this optimum value, the negative influence overcomes the positive impact.

4.5. Mechanical limitations on the rollers diameter

Based on the DEM results, reducing the rollers diameter leads to increasing the efficiency of the device, however, such a modification causes mechanical weakening and increases the probability of permanent bending deformation of the rollers. In order to

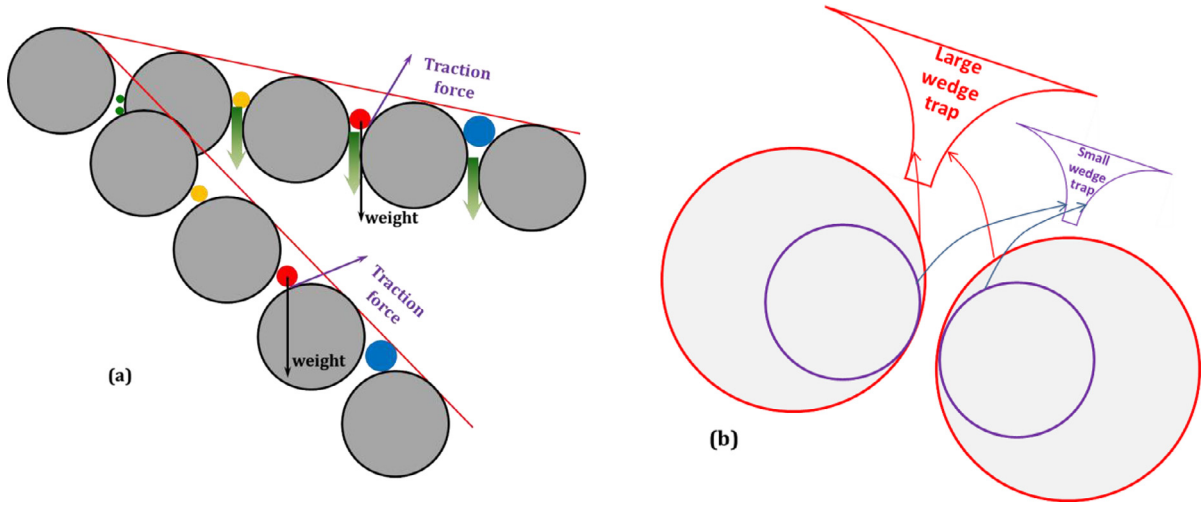

Fig. 17. Physical explanation effects of the deck angle on the opening area and the highest attainable efficiency versus the rollers diameter and associated optimum speed.

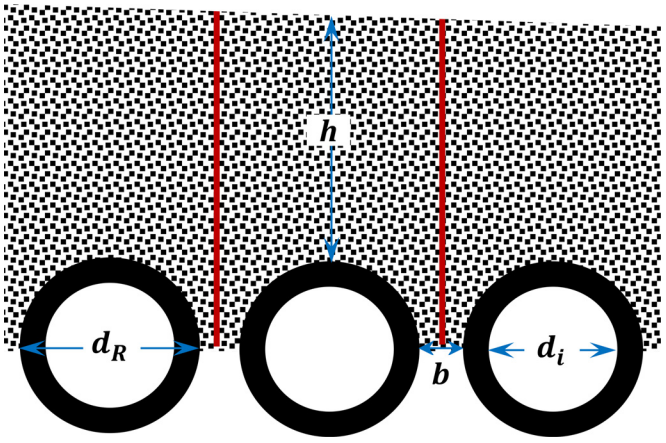

Fig. 18. Schematic section view of the stacked pellets on the screen causing distributed load along the rollers.

investigate this issue, parametric relationships to calculate maximum stress and maximum deflection of the rollers are developed using the beam theory. Normally, the load on each roller includes its own weight and the weight of the stacked pellets on the screen. As shown in Fig. 18, the distributed load on each roller can be determined in terms of its inner and outer diameter, the gap between the rollers, and the height of the stacked pellets.

The weight of a roller depends on its weight density, internal and external diameters; and its uniform load intensity (force per unit length) is determined from the following equation.

$$W_R = \rho_R g \frac{\pi}{4}\left(d_R^2 - d_i^2\right) \tag{11}$$

In the above equation, g is the gravitational acceleration, and ρ_R, d_R and $d_i$are weight density, outer diameter and inner diameter of the roller, respectively. On the other hand, uniform load intensity due to the pellet weight on each roller is determined from the following equation.

$$W_P = \rho_{P'} g h (d_o + b) \tag{12}$$

In this equation, $\rho_{P'}$ is overall density of the stacked pellets, which due to the empty spaces between them is less than the density of a single pellet. However, for simplicity and also in order to enhance the design safety, this value is also selected equal to the pellet density, ($\rho_{P'} \cong \rho_P$). As indicated in Fig. 18, h is the height of the pellets stacked on the screen and b is the gap between the rollers. Assuming simple support bearings on both sides of the rollers, maximum deflection and maximum normal stress at the midpoint section of the rollers are determined via the following equations Budynas and Nisbett, 2022). In these equations, W is the total load intensity which is the summation of the roller weight and pellets weight already introduced in Eqs. (11) and (12).

$$\delta_{max} = \frac{5WL^4}{384E_R I} \tag{13}$$

$$\sigma_{max} = \frac{W d_R L^2}{16I} \tag{14}$$

In the above, E_R is Young's modulus, $I = \frac{\pi}{64}(d_R^4 - d_i^4)$is the second moment of inertia of the roller cross section and $L$is the roller length. By combining the above Eqs. with Eqs. (11) and (12), the following results are obtained to calculate the maximum deflection and maximum normal stress, respectively. In fact, the first term in these equations is due to the weight of the roller and the second term refers to the weight of the stacked pellets.

$$\delta_{max} = \frac{5gL^4\rho_R}{24E_R\left(d_o^2 + d_i^2\right)} + \frac{5gL^4\rho_P h(d_o + b)}{6E_R\pi\left(d_o^4 - d_i^4\right)} \tag{15}$$

$$\sigma_{max} = \frac{g d_o L^2 \rho_R}{\left(d_o^2 + d_i^2\right)} + \frac{4g d_o L^2 \rho_P h(d_o + b)}{\pi\left(d_o^4 - d_i^4\right)} \tag{16}$$

Using these parametric equations, maximum deflection and maximum stress can be compared under different conditions. As a general realistic case, the rollers are made of steel and the problem characteristics are: $\rho_R = 7800$ kg/m^3, $E_R = 200$ GPa, $L = 4$ m, $\rho_p = 3150$ kg/m^3, $b = 16$ mm. According to DEM results and also as observed in the real conditions, the height of the pellets from its maximum around 300 mm at the charge gate approaches to a tiny thickness at the end of the screen deck. Maximum stress and deflection of the rollers versus the outer and inner diameter of the rollers and for different values of the pellets load height are plotted in Fig. 19. It is realized that in all values of the outer diameter with decreasing the inner diameter, values of deflection and stress decrease. Nevertheless, this behavior is such that when the inner diameter is smaller than a limit, which is called optimal limit here, the graphs become almost plateau. The reason for this manner is the presence of the diameter in degrees of fourth and second at the denominator of the deflection and stress Eqs. (15) and (16). In other words, the central region of the rollers cross section does not have a significant impact on its strength and hence it is reasonable to be made as hollow tube.

In terms of screening, DEM results proved that the efficiency growths with decreasing the diameter of the rolls, on the other hand, here is revealed that reducing the diameter leads to amplification in the stress and deflection of the rollers. From a mechanical viewpoint, the maximum deflection and maximum stress must be less than their relevant allowable limits. According to the stress design criterion, maximum stress must be less than the fatigue endurance limit of the roller material (Budynas and Nisbett, 2022). Therefore, mechanical strength of the roller material is a key factor in this issue. It is worth mentioning the fact that the fatigue strength of most conventional alloy steels in roller construction is more than 200 MPa. On the other hand, no definite index and standard have been seen in the open literature for allowable deflection of the rollers. As a practical approach to predict allowable limits of the deflection and stress, an inverse method can be implemented by using the on-site real condition. To explain this approach, a realistic example is studied in which the outer and inner diameters of the rollers are: $d_R = 85$ mm and $d_i = 50$ mm. Based on the graphs in Fig. 19 in case that $h = 300$ mm, maximum deflection and stress are 9 mm and 46 MPa, respectively. In reality, this load height was present on the rollers at the beginning of the device and they did not show any mechanical problem and hence, 9 mm and 46 MPa can be considered in allowable ranges of the deflection and stress, respectively. For the same example, the height of the real stacked pellets in the middle zone onwards reaches approximately 100 mm and less. The graphs in Fig. 19 show that at such position, the maximum deflection and stress are 4.5 mm and 23 MPa, respectively, which are much less than the introduced allowable limits. Thus, the diameter of the rollers located within the last half of the screen can be safely reduced to such an extent that for a load height of $h = 100$ mm, their deflection and stress do not exceed 9 mm and 46 MPa, respectively. With these explanations, by referring to the graphs in Fig. 19 the outer diameter of these rollers can be reduced to 65 mm while their inner diameter is 40 mm. In this case, maximum deflection and stress become about 9 mm and 35 MPa, respectively, which are still less than the corresponding values that occurred for the larger rollers at the beginning of the device.

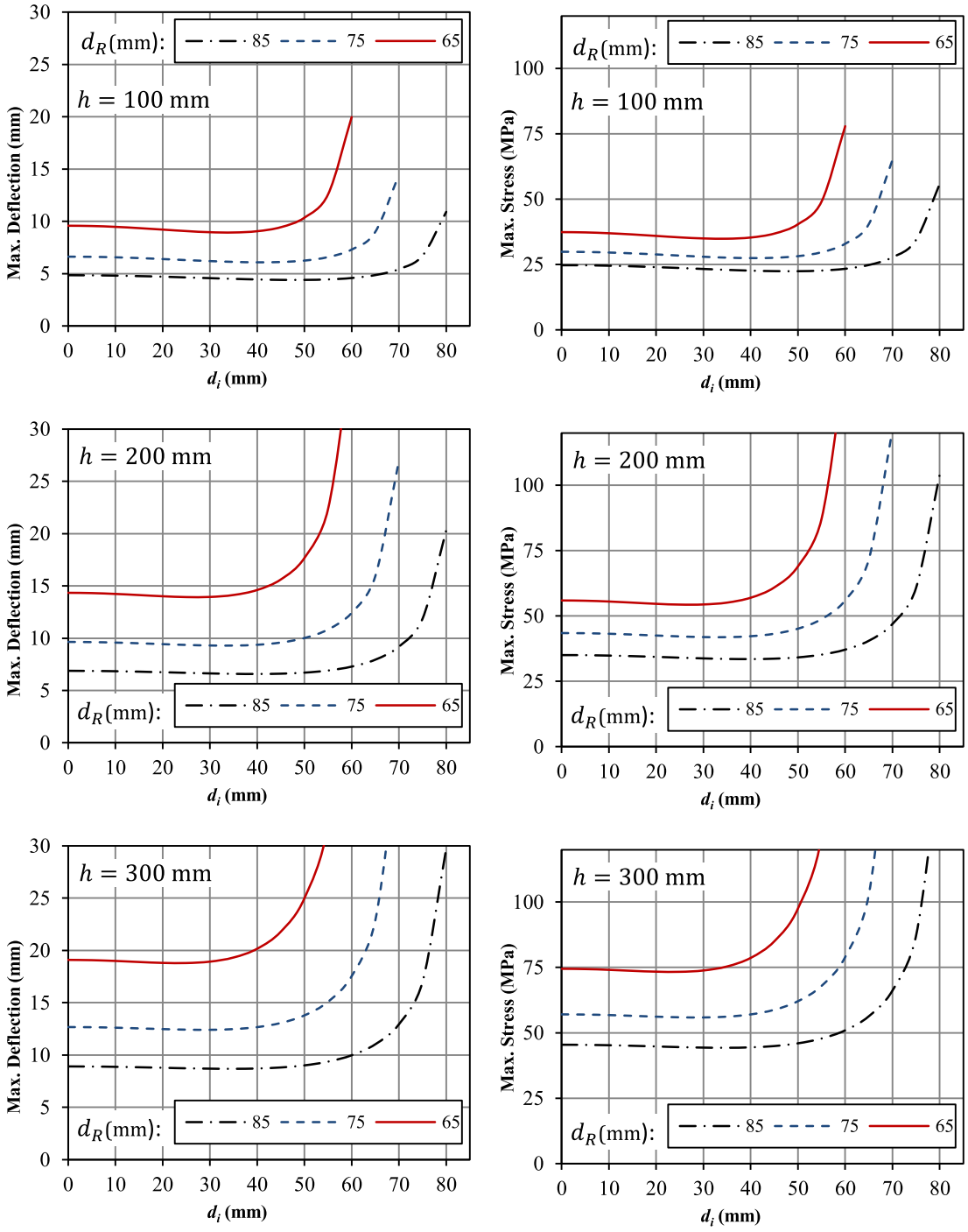

Fig. 19. Graphs of maximum deflection and normal stress versus inner and outer diameter of the roller for different values of the stacked pellets height.

5. Concluding remarks

In this paper, we explained the strategy of simulating the roller screen via DEM. JKR model was used to determine the contact force. It was seen that the accuracy of the results depends on the meshing of the rollers surface, time step size, and grid size. Accordingly, suitable values of these parameters were selected based on sensitivity analysis. Via the simulation of several problems with different conditions, the effects of the rollers diameter, rollers speed and deck angle on the local and total underflow rate, efficiency and cooperation index were studied. Based on the obtained results, the increase in the rollers diameter reduced the efficiency. It was further revealed that through the rise in the deck angle, the efficiency decreases; however, the trend depends on the rollers speed and rollers diameter. It was concluded that by increasing the rollers speed to an optimum value, the efficiency rises and is then reduced beyond that limit. In other words, for a specific set of values of the rollers diameter and deck angle, their speed should be at an optimum value to achieve the maximum attainable efficiency. It was further revealed that the optimum speed depends on both the rollers diameter and deck angle.

- The physical illustration of the impact of the rollers speed can be summarized as:

Increase in the rollers speed reduces the time that the pellets retain on the screen, and decline in the chance of the undersized pellets to pass through the gaps diminishes the efficiency. On the other hand, increasing the rollers speed enhances the power of the traction force on the pellets, assisting them to go out of the wedge trap between the rollers. However, this effect happens for all pellets and not just the oversize ones. Combining these two opposite effects of the rollers speed leads to the formation of an optimum point in the relationship between the efficiency and the rollers speed.

- Physical explanation regarding effect of the deck angle on the efficiency can be summarized as follows:

The rise in the deck angle reduces the projection of the openings width along the horizon, thereby decreasing the effective opening area. Furthermore, the increase in the deck angle augments the contribution of the pellets weight on the front roller of each adjacent pair of rollers leading to boost the traction that cause pellets transfer along the screen deck. Accordingly, the passage probability of the near undersized (critical degree 3) and even too undersized (critical degree 1) pellets is reduced, leading to efficiency degradation. Although the increase in the deck angle weakens the efficiency, this negative effect can be compensated by decreasing the rollers speed.

- From a physical viewpoint, the effects of the rollers diameter on the efficiency and mechanical considerations can be summarized as follows:

With the decrease in the rollers diameter, the number of openings obviously increases resulting in an increase in the effective screen area and thus higher efficiency. Furthermore, the wedge shape trap between each pair of rollers is contracted, causing less trouble for transferring the near oversized pellets. Additionally, as the wedge trap is contracted, a lower number of near oversized pellets stay inside it and the probability of blinding decreases accordingly. Although the decrease in the rollers diameter causes an increase in the screening efficiency, the rollers are weakened in a mechanical viewpoint. Here, a parametric study was conducted to reveal the dependencies of the stress and deflection of the rollers on the problem characteristics. The proposed approach was implemented in a practical example to observe how the rollers diameter can be reduced in order to increase the device efficiency while mechanical strength limits were also taken into account to avoid permanent bending.

Declaration of Competing Interest

The authors whose names are listed immediately below certify that they have NO conflict of interest and NO affiliations with or involvement in any organization or entity with any financial interest (such as honoraria; educational grants; participation in speakers' bureaus; membership, employment, consultancies, stock ownership, or other equity interest; and expert testimony or patent-licensing arrangements), or non-financial interest (such as personal or professional relationships, affiliations, knowledge or beliefs) in the subject matter or materials discussed in this manuscript.

CRediT authorship contribution statement

Akbar Jafari: Visualization, Conceptualization, Investigation, Formal analysis, Writing – original draft. **Meisam Javaheri:** Visualization, Conceptualization, Investigation, Formal analysis, Writing – original draft. **Gholamhosein Baradaran:** Visualization, Conceptualization, Investigation, Formal analysis, Writing – original draft.

Acknowledgment

We acknowledge the financial support from Iran Natural Science Foundation (INSF) under grant No. 93038047.

References

Baran, O., DeGennaro, A., Ramé, E., Wilkinson, A., 2009. DEM simulation of a schulze ring shear tester. AIP Conf. Proc. 1145, 409–412.
Budynas, R., Nisbett, K., 2022. Shigley's Mechanical Engineering Design. McGraw-Hill.
Cleary, P.W., 2010. DEM prediction of industrial and geophysical particle flows. Particuology 8, 106–118.
Cleary, P.W., 2019. Effect of rock shape representation in DEM on flow and energy utilisation in a pilot SAG mill. Comput. Part. Mech. 6, 461–477.
Cundall, P.A., Strack, O.D., 1979. A discrete numerical model for granular assemblies. Geotechnique 29, 47–65.
Danby, M., Shrimpton, J., Palmer, M., 2013. On the optimal numerical time integration for DEM using Hertzian force models. Comput. Chem. Eng. 58, 211–222.
e Silva, B.B., da Cunha, E.R., de Carvalho, R.M., Tavares, L.M., 2018. Modeling and simulation of green iron ore pellet classification in a single deck roller screen using the discrete element method. Powder Technol. 332, 359–370.
e Silva, B.B., da Cunha, E.R., de Carvalho, R.M., Tavares, L.M., 2020. Improvement in roller screening of green iron ore pellets by statistical analysis and discrete element simulations. Miner. Process. Extr. Metall. Rev. 41, 323–334.
EDEM, 2018. EDEM User Guide. DEM Solutions, Edinburgh.www.dem-solutions.com.
Geleta, D.D., Lee, J., 2018. Effects of particle diameter and coke layer thickness on solid flow and stress distribution in BF by 3D discrete element method. Metall. Mater. Trans. B 49, 3594–3602.
Ghodki, B.M., Patel, M., Namdeo, R., Carpenter, G., 2019. Calibration of discrete element model parameters: soybeans. Comput. Part. Mech. 6, 3–10.
Halt, J.A., Silva, B.B., Kawatra, S.K., 2015. A new on-line method for predicting iron ore pellet quality. Miner. Process. Extr. Metall. Rev. 36, 377–384.
Hamzeloo, E., Massinaei, M., Mehrshad, N., 2014. Estimation of particle size distribution on an industrial conveyor belt using image analysis and neural networks. Powder Technol. 261, 185–190.
He, Y., Evans, T.J., Shen, Y.S., Yu, A.B., Yang, R.Y., 2018. Discrete modelling of the compaction of non-spherical particles using a multi-sphere approach. Miner. Eng. 117, 108–116.
Heydari, M., Amirfattahi, R., Nazari, B., Rahimi, P., 2016. An industrial image processing-based approach for estimation of iron ore green pellet size distribution. Powder Technol. 303, 260–268.
Hyvärinen, M., Ronkanen, M., Kärki, T., 2020. Sorting efficiency in mechanical sorting of construction and demolition waste. Waste Manag. Res. 38, 812–816.
Jafari, A., Abbasi Hattani, R., 2020. Investigation of parameters influencing erosive wear using DEM. Friction 8, 136–150.
Jafari, A., Saljooghi Nezhad, V., 2016. Employing DEM to study the impact of different parameters on the screening efficiency and mesh wear. Powder Technol. 297, 126–143.
Javaheri, M., Jafari, A., Baradaran, G.H., Saidi, A., 2021. Effects of rollers speed regime on the roller screen efficiency. Miner. Process. Extr. Metall. Rev. 1–8.
Johnson, K.L., Kendall, K., Roberts, A.D., 1971. Surface energy and the contact of elastic solids. Proc. R. Soc. Lond. A 324, 301–313.
Kotta, A.B., Patra, A., Kumar, M., Karak, S.K., 2019. Effect of molasses binder on the physical and mechanical properties of iron ore pellets. Int. J. Miner. Metall. Mater. 26, 41–51.
Kruggel-Emden, H., Sturm, M., Wirtz, S., Scherer, V., 2008. Selection of an appropriate time integration scheme for the discrete element method (DEM). Comput. Chem. Eng. 32, 2263–2279.
Liu, S., Wang, Y., Shen, C., 2018. DEM analysis of granular crushing during simple shearing. Mar. Georesources Geotechnol. 36, 522–531.
Mishra, B.K., Thornton, C., Bhimji, D., 2002. A preliminary numerical investigation of agglomeration in a rotary drum. Miner. Eng. 15, 27–33.
Nyembwe, A.M., Cromarty, R.D., Garbers-Craig, A.M., 2017. Relationship between iron ore granulation mechanisms, granule shapes, and sinter bed permeability. Miner. Process. Extr. Metall. Rev. 38, 388–402.
O'Sullivan, C., Bray Jonathan, D., 2004. Selecting a suitable time step for discrete element simulations that use the central difference time integration scheme. Eng. Comput. 21, 278–303.
Powell, M.S., Weerasekara, N.S., Cole, S., LaRoche, R.D., Favier, J., 2011. DEM modelling of liner evolution and its influence on grinding rate in ball mills. Miner. Eng. 24, 341–351.
Sofu, M.M., Er, O., Kayacan, M.C., Cetişli, B., 2016. Design of an automatic apple sorting system using machine vision. Comput. Electron. Agric. 127, 395–405.
Solutions, D. (2018). EDEM user guide. In. Edinburgh, UK.
Tavares, L.M., 2017. A review of advanced ball mill modelling. KONA Powder Part. J. 34, 106–124.
Technical report: Application of image processing to improve performance of pelletizing disks, 2019. Department of research and development, Golgohar mining and industrial complex, http://www.geg.ir/.

Tupkary, R.H., Tupkary, V.R., 2013. An Introduction to Modern Iron Making. Khanna Publishers Pvt. Ltd, New Delhi, India.
Wang, Z., Peng, L., Zhang, C., Qi, L., Liu, C., Zhao, Y., 2019. Research on impact characteristics of screening coals on vibrating screen based on discrete-finite element method. Energy Sources Part A Recovery Util. Environ. Eff. 42 (16), 1–14.
Yang, W., Zhou, Z., Pinson, D., Yu, A., 2015. A New approach for studying softening and melting behavior of particles in a blast furnace cohesive zone. Metall. Mater. Trans. B 46, 977–992.
Yang, X.D., Zhao, L.L., Li, H.X., Liu, C.S., Hu, E.Y., Li, Y.W., Hou, Q.F., 2020. DEM study of particles flow on an industrial-scale roller screen. Adv. Powder Technol. 31, 4445–4456.
Yu, Y., Zhang, J., Zhang, J., Saxén, H., 2018. DEM and experimental studies on pellet segregation in stockpile build-up. Ironmak. Steelmak. 45, 264–271.